Hyperon stars in a modified quark meson coupling model

R. N. Mishra,[1] H. S. Sahoo,[1] P. K. Panda,[2] N. Barik,[2] and T. Frederico[3]
[1]*Department of Physics, Ravenshaw University, Cuttack-753 003, India*
[2]*Department of Physics, Utkal University, Bhubaneswar-751 004, India*
[3]*Instituto Tecnólogico de Aeronática, DCTA, 12228-900 São José dos Campos, SP, Brazil*
(Received 28 June 2016; revised manuscript received 4 August 2016; published 23 September 2016)

We determine the equation of state (EOS) of nuclear matter with the inclusion of hyperons in a self-consistent manner by using a modified quark meson coupling model where the confining interaction for quarks inside a baryon is represented by a phenomenological average potential in an equally mixed scalar-vector harmonic form. The hadron-hadron interaction in nuclear matter is then realized by introducing additional quark couplings to σ, ω, and ρ mesons through mean-field approximations. The effect of a nonlinear ω-ρ term on the EOS is studied. The hyperon couplings are fixed from the optical potential values and the mass-radius curve is determined satisfying the maximum mass constraint of 2 $M_\odot$ for neutron stars, as determined in recent measurements of the pulsar PSR J0348+0432. We also observe that there is no significant advantage of introducing the nonlinear ω-ρ term in the context of obtaining the star mass constraint in the present set of parametrizations.

DOI: 10.1103/PhysRevC.94.035805

I. INTRODUCTION

Over the last few decades intensive theoretical investigations have been pursued to understand the microscopic composition and properties of dense nuclear matter. It has been realized by now from such studies [1–9] that high density nuclear matter may consist not only of nucleons and leptons but also several exotic components such as hyperons, mesons, as well as quark matter in different forms and phases. Hyperons in particular are expected to appear in the inner core of neutron stars at densities 2–3 times the normal saturation density $\rho_0 = 0.15$ fm^{-3}. This is because at such high densities the nucleon chemical potential becomes large enough to facilitate the formation of hyperons to be energetically favorable by the inverse β decay process of nucleons in the β-stable nuclear matter. As a consequence the Fermi pressure exerted by the baryons is reduced and the equation of state (EOS) describing such dense matter in neutron stars with hyperon core becomes softer leading to the reduction of the maximum mass of the star [10–15]. However relativistic Hartree-Fock models [16,17], relativistic mean field models [18,19], or quantum hadrodynamic model [20] show relatively weaker effects on the EOS due to the presence of strange baryons in the neutron star core.

Until recently the reliability requirement for any model EOS was only to predict a maximum neutron star mass $M_{\rm max}$ compatible with the canonical value of 1.4–1.5 $M_\odot$, since most of the precisely measured neutron star mass were clustered around these values only. This constraint was probably not stringent enough for which without any discrimination, most relativistic models even with the inclusion of hyperons [10–14] have succeeded to this extent. But recent discovery of the unusually high mass of the millisecond pulsars PSR J1903+0327 (1.66 ± 0.021 $M_\odot$) [21–23], PSR J1614-2230 (1.97 ± 0.04 $M_\odot$) [24], and PSR J0348+0432 (2.01 ± 0.04 $M_\odot$) [25] show that the neutron star mass distribution is much wider extending firmly up to 1.9–2.0 $M_\odot$. Also there has been considerable progress in the measurement of the neutron star radii by reducing their uncertainties with a better understanding of the sources of systematic errors to estimate them in 10.1–11.1 km range for a 1.5 $M_\odot$ neutron star [26]. Another study by Fortin *et al.* [27] has shown that the observational constraint on the maximum mass implies that the hyperonic stars with masses in the range 1–1.6 $M_\odot$ must be larger than 13 km due to a prehyperonic stiffening of EOS. It has been found by Providência and Rabhi [28] that the radius of a hyperonic star of a given mass decreases linearly with the increase of the total hyperon content. These observations may serve to further constrain the EOS in achieving greater reliability.

Various studies have established that the presence of hyperons in the neutron star core leads to softening of the EOS and consequent reduction in the maximum mass of the star. This has provided a challenge to develop an equation of state (EOS) stiff enough to give such high mass with the inclusion of hyperons. In fact most relativistic models obtain maximum star masses in the range 1.4–1.8$M_\odot$ with the inclusion of hyperons [11]. However there are some exceptional cases [29] where maximum mass of the hyperonic star have been realized in the range 1.8–2.1 $M_\odot$.

In the present work, we have developed an EOS using a modified quark-meson coupling (MQMC) model. The MQMC model is based on confining relativistic independent quark potential model rather than a bag to describe the baryon structure in vacuum. In such a picture the quarks inside the baryon are considered to be independently confined by a phenomenologically average potential with an equally mixed scalar-vector harmonic form. Such a potential has characteristically simplifying features in converting the independent quark Dirac equation into a Schrödinger-like equation for the upper component of Dirac spinor which can be solved easily. The implications of such potential forms in the Dirac framework has been studied earlier [30,31]. The baryon-baryon interactions are realized by making additional quark couplings to σ, ω, and ρ mesons through mean-field approximations, in an extension of previous works based on the MIT bag model [32–34]. The MQMC model has already been well

tested in determining various bulk properties of symmetric and asymmetric nuclear matter [35,36]. The relevant parameters of the interaction are obtained self-consistently by realizing the saturation properties such as binding energy and pressure. Here, we study the role of hyperons on the properties of neutron stars. In the present work we have also introduced an additional nonlinear ω-ρ coupling to study its effect on the stiffening of EOS necessary for the purpose.

We include hyperons as a new degree of freedom in dense hadronic matter relevant for neutron stars. The interactions between nucleons and the baryons of the baryon octet in dense matter is studied and its effects on the mass of the neutron star is analyzed. The nucleon-nucleon interaction is well known from nuclear properties. But the extrapolation of such interactions to densities beyond nuclear saturation density is a great problem. Most of the hyperon-nucleon interaction are known experimentally. This has inspired us to set the hyperon-nucleon interaction potential at saturation density for the Λ, Σ, and Ξ hyperons to $U_\Lambda = -28$ MeV, $U_\Sigma = 30$ MeV, and $U_\Xi = -18$ MeV, respectively. Because of the uncertainties in the measurement of the Ξ hyperon potentials, we make a variation in the U_Ξ and study the effects on the mass of the star. However, we do not include the hyperon-hyperon interactions which are experimentally least well known.

In this model we observe that the compressibility of the neutron star matter depends on the mass of the quark. The quark mass has been fixed at 150 MeV giving us a compressibility of 292 MeV which lies within the range predicted from experimental GMR studies [37] and also from theoretical predictions of infinite nuclear matter model [38]. We also compare our results at two different quark masses of $m_q = 150$ MeV and $m_q = 80$ MeV.

The paper is organized as follows. In Sec. II, a brief outline of the model describing the baryon structure in vacuum is discussed. The baryon mass is then realized by appropriately taking into account the center-of-mass correction, pionic correction, and gluonic correction in Sec. III. The EOS is then developed in Sec. IV. The results and discussions are made in Sec. V. We summarize our findings in Sec. IV.

II. MODIFIED QUARK MESON COUPLING MODEL

The modified quark-meson coupling model has been extensively applied for the study of the bulk properties of both symmetric as well as asymmetric nuclear matter. Under such a model the nucleon-nucleon (NN) interaction was realized in a mean-field approach through the exchange of effective (σ,ω) mesonic fields coupling to the quarks inside the nucleon for the symmetric case [35] and the additional isovector-vector meson field (ρ) coupling to the quarks for the asymmetric case [36]. In our earlier work [36] this model was used to investigate the nature of the thermodynamic instabilities and the correlation of the symmetry energy with its slope. We now extend this model to investigate the role of nucleons and hyperons in neutron star matter under conditions of β equilibrium and charge neutrality.

We begin by considering baryons as composed of three constituent quarks in a phenomenological flavor-independent confining potential, $U(r)$ in an equally mixed scalar and vector harmonic form inside the baryon [35], where

$$U(r) = \tfrac{1}{2}(1+\gamma^0)V(r)$$

with

$$V(r) = (ar^2 + V_0), \qquad a > 0. \tag{1}$$

Here (a, V_0) are the potential parameters. The confining interaction provides the zeroth-order quark dynamics of the hadron. In the medium, the quark field $\psi_q(\mathbf{r})$ satisfies the Dirac equation

$$\left[\gamma^0\left(\epsilon_q - V_\omega - \frac{1}{2}\tau_{3q}V_\rho\right) - \vec{\gamma}.\vec{p} - (m_q - V_\sigma) - U(r)\right] \times \psi_q(\vec{r}) = 0, \tag{2}$$

where $V_\sigma = g^q_\sigma\sigma_0$, $V_\omega = g^q_\omega\omega_0$, and $V_\rho = g^q_\rho b_{03}$. Here σ_0, ω_0, and b_{03} are the classical meson fields, and g^q_σ, g^q_ω, and g^q_ρ are the quark couplings to the σ, ω, and ρ mesons, respectively. m_q is the quark mass and τ_{3q} is the third component of the Pauli matrices. We can now define

$$\epsilon'_q = (\epsilon^*_q - V_0/2) \quad \text{and} \quad m'_q = (m^*_q + V_0/2), \tag{3}$$

where the effective quark energy, $\epsilon^*_q = \epsilon_q - V_\omega - \frac{1}{2}\tau_{3q}V_\rho$ and effective quark mass, $m^*_q = m_q - V_\sigma$. We now introduce λ_q and r_{0q} as

$$(\epsilon'_q + m'_q) = \lambda_q \quad \text{and} \quad r_{0q} = (a\lambda_q)^{-\frac{1}{4}}. \tag{4}$$

The ground-state quark energy can be obtained from the eigenvalue condition

$$(\epsilon'_q - m'_q)\sqrt{\frac{\lambda_q}{a}} = 3. \tag{5}$$

The solution of Eq. (5) for the quark energy ϵ^*_q immediately leads to the mass of baryon in the medium in zeroth order as

$$E^{*0}_B = \sum_q \epsilon^*_q. \tag{6}$$

III. EFFECTIVE MASS OF BARYON

We next consider the spurious center-of-mass correction $\epsilon_{c.m.}$, the pionic correction δM^π_B for restoration of chiral symmetry, and the short-distance one-gluon exchange contribution $(\Delta E_B)_g$ to the zeroth-order baryon mass in the medium.

Here, we extract the center of mass energy to first order in the difference between the fixed center and relative quark co-ordinate, using the method described by Guichon *et al.* [32]. The center of mass correction is given by

$$e_{\text{c.m.}.} = e^{(1)}_{\text{c.m.}} + e^{(2)}_{\text{c.m.}}, \tag{7}$$

where

$$e^{(1)}_{\text{c.m.}} = \sum_{i=1}^{3}\left[\frac{m_{q_i}}{\sum_{k=1}^{3} m_{q_k}}\frac{6}{r^2_{0q_i}\left(3\epsilon'_{q_i} + m'_{q_i}\right)}\right], \tag{8}$$

$$e^{(2)}_{\rm c.m.} = \frac{a}{2}\Bigg[\frac{2}{\sum_k m_{q_k}}\sum_i m_i\langle r_i^2\rangle + \frac{2}{\sum_k m_{q_k}}\sum_i m_i\langle\gamma^0(i)r_i^2\rangle - \frac{3}{\left(\sum_k m_{q_k}\right)^2}\sum_i m_i^2\langle r_i^2\rangle$$
$$- \frac{1}{\left(\sum_k m_{q_k}\right)^2}\sum_i\langle\gamma^0(1)m_i^2r_i^2\rangle - \frac{1}{\left(\sum_k m_{q_k}\right)^2}\sum_i\langle\gamma^0(2)m_i^2r_i^2\rangle - \frac{1}{\left(\sum_k m_{q_k}\right)^2}\sum_i\langle\gamma^0(3)m_i^2r_i^2\rangle\Bigg]. \quad (9)$$

In the above, we have used for $i = (u,d,s)$ and $k = (u,d,s)$ and the various quantities are defined as

$$\langle r_i^2\rangle = \frac{(11\epsilon'_{qi} + m'_{qi})r_{0qi}^2}{2(3\epsilon'_{qi} + m'_{qi})}, \quad (10)$$

$$\langle\gamma^0(i)r_i^2\rangle = \frac{(\epsilon'_{qi} + 11m'_{qi})r_{0qi}^2}{2(3\epsilon'_{qi} + m'_{qi})}, \quad (11)$$

$$\langle\gamma^0(i)r_j^2\rangle_{i\neq j} = \frac{(\epsilon'_{qi} + 3m'_{qi})\langle r_j^2\rangle}{3\epsilon'_{qi} + m'_{qi}}. \quad (12)$$

The pseudovector nucleon pion coupling constant, $f_{NN\pi}$ can be obtained from Goldberg-Treiman relations by using the axial-vector coupling constant value g_A in the model as

$$\sqrt{4\pi}\frac{f_{NN\pi}}{m_\pi} = \frac{g_A(N)}{2f_\pi}, \quad (13)$$

where

$$g_A(n \to p) = \frac{5}{9}\frac{(5\epsilon'_u + 7m'_u)}{(3\epsilon'_u + m'_u)}. \quad (14)$$

The pionic corrections in the model for the nucleons become

$$\delta M_N^\pi = -\frac{171}{25} I_\pi f_{NN\pi}^2. \quad (15)$$

Taking $w_k = (k^2 + m_\pi^2)^{1/2} I_\pi$ becomes

$$I_\pi = \frac{1}{\pi {m_\pi}^2}\int_0^\infty dk.\frac{k^4u^2(k)}{w_k^2} \quad (16)$$

with the axial vector nucleon form factor given as

$$u(k) = \Big[1 - \frac{3}{2}\frac{k^2}{\lambda_q(5\epsilon'_q + 7m'_q)}\Big]e^{-k^2r_0^2/4}. \quad (17)$$

The pionic correction for Σ^0 and Λ^0 becomes

$$\delta M_{\Sigma^0}^\pi = -\frac{12}{5} f_{NN\pi}^2 I_\pi, \quad (18)$$

$$\delta M_{\Lambda^0}^\pi = -\frac{108}{25} f_{NN\pi}^2 I_\pi. \quad (19)$$

Similarly the pionic correction for Σ^- and Σ^+ is

$$\delta M_{\Sigma^+,\Sigma^-}^\pi = -\frac{12}{5} f_{NN\pi}^2 I_\pi. \quad (20)$$

The pionic correction for Ξ^0 and Ξ^- is

$$\delta M_{\Xi^-,\Xi^0}^\pi = -\frac{27}{25} f_{NN\pi}^2 I_\pi. \quad (21)$$

The one-gluon exchange interaction is provided by the interaction Lagrangian density

$$\mathcal{L}_I^g = \sum J_i^{\mu a}(x)A_\mu^a(x), \quad (22)$$

where $A_\mu^a(x)$ are the octet gluon vector-fields and $J_i^{\mu a}(x)$ is the ith quark color current. The gluonic correction can be separated in two pieces, namely, one from the color electric field (E_i^a) and another from the magnetic field (B_i^a) generated by the ith quark color current density

$$J_i^{\mu a}(x) = g_c\bar\psi_q(x)\gamma^\mu\lambda_i^a\psi_q(x) \quad (23)$$

with λ_i^a being the usual Gell-Mann $SU(3)$ matrices and $\alpha_c = g_c^2/4\pi$. The contribution to the mass can be written as a sum of color electric and color magnetic part as

$$(\Delta E_B)_g = (\Delta E_B)_g^E + (\Delta E_B)_g^M, \quad (24)$$

where

$$(\Delta E_B)_g^E = \frac{1}{8\pi}\sum_{i,j}\sum_{a=1}^{8}\int\frac{d^3r_id^3r_j}{|r_i - r_j|} \times \langle B|J_i^{0a}(r_i)J_j^{0a}(r_j)|B\rangle, \quad (25)$$

and

$$(\Delta E_B)_g^M = -\frac{1}{8\pi}\sum_{i,j}\sum_{a=1}^{8}\int\frac{d^3r_id^3r_j}{|r_i - r_j|} \times \langle B|\vec J_i^a(r_i)\vec J_j^a(r_j)|B\rangle. \quad (26)$$

Finally, taking into account the specific quark flavor and spin configurations in the ground state baryons and using the relations $\langle\sum_a(\lambda_i^a)^2\rangle = 16/3$ and $\langle\sum_a(\lambda_i^a\lambda_j^a)\rangle_{i\neq j} = -8/3$ for baryons, one can write the energy correction due to color electric contribution, as

$$(\Delta E_B)_g^E = \alpha_c\left(b_{uu}I_{uu}^E + b_{us}I_{us}^E + b_{ss}I_{ss}^E\right), \quad (27)$$

and due to color magnetic contributions, as

$$(\Delta E_B)_g^M = \alpha_c\left(a_{uu}I_{uu}^M + a_{us}I_{us}^M + a_{ss}I_{ss}^M\right), \quad (28)$$

where a_{ij} and b_{ij} are the numerical coefficients depending on each baryon and are given in Table I. In the above, we have

$$I_{ij}^E = \frac{16}{3\sqrt{\pi}}\frac{1}{R_{ij}}\Big[1 - \frac{\alpha_i + \alpha_j}{R_{ij}^2} + \frac{3\alpha_i\alpha_j}{R_{ij}^4}\Big],$$
$$I_{ij}^M = \frac{256}{9\sqrt{\pi}}\frac{1}{R_{ij}^3}\frac{1}{(3\epsilon_i^{'} + m_i^{'})}\frac{1}{(3\epsilon_j^{'} + m_j^{'})}, \quad (29)$$

TABLE I. The coefficients a_{ij} and b_{ij} used in the calculation of the color-electric and and color-magnetic energy contributions due to one-gluon exchange.

Baryon	a_{uu}	a_{us}	a_{ss}	b_{uu}	b_{us}	b_{ss}
N	−3	0	0	0	0	0
Λ	−3	0	0	1	−2	1
Σ	1	−4	0	1	−2	1
Ξ	0	−4	1	1	−2	1

where

$$R_{ij}^2 = 3\left[\frac{1}{\left(\epsilon_i^{'2} - m_i^{'2}\right)} + \frac{1}{\left(\epsilon_j^{'2} - m_j^{'2}\right)}\right],$$
$$\alpha_i = \frac{1}{(\epsilon_i^{'} + m_i^{'})(3\epsilon_i^{'} + m_i^{'})}. \tag{30}$$

The color electric contributions to the bare mass for nucleon $(\Delta E_N)_g^E = 0$. Therefore the one-gluon contribution for nucleon becomes

$$(\Delta E_N)_g^M = -\frac{256\alpha_c}{3\sqrt{\pi}}\left[\frac{1}{(3\epsilon_u' + m_u')^2 R_{uu}^3}\right]. \tag{31}$$

The one-gluon contribution for Σ^+, Σ^- becomes

$$(\Delta E_{\Sigma^+,\Sigma^-})_g^E = \alpha_c \frac{16}{3\sqrt{\pi}}\left[\frac{1}{R_{uu}}\left(1 - \frac{2\alpha_u}{R_{uu}^2} - \frac{3\alpha_u^2}{R_{uu}^4}\right) - \frac{2}{R_{us}}\left(1 - \frac{\alpha_u + \alpha_s}{R_{us}^2} + \frac{3\alpha_u\alpha_s}{R_{us}^4}\right) + \frac{1}{R_{ss}}\left(1 - \frac{2\alpha_s}{R_{ss}^2} + \frac{3\alpha_s^2}{R_{ss}^4}\right)\right], \tag{32}$$

$$(\Delta E_{\Sigma^+,\Sigma^-})_g^M = \frac{256\alpha_c}{9\sqrt{\pi}}\left[\frac{1}{(3\epsilon_u' + m_u')^2 R_{uu}^3} - \frac{4}{R_{us}^3(3\epsilon_u' + m_u')(3\epsilon_s' + m_s')}\right], \tag{33}$$

$$(\Delta E_{\Sigma^+,\Sigma^-})_g = (\Delta E_{\Sigma^+,\Sigma^-})_g^E + (\Delta E_{\Sigma^+,\Sigma^-})_g^M. \tag{34}$$

The gluonic correction for Σ^0 is

$$(\Delta E_{\Sigma^0})_g^E = \alpha_c \frac{16}{3\sqrt{\pi}}\left[\frac{1}{R_{uu}}\left(1 - \frac{2\alpha_u}{R_{uu}^2} - \frac{3\alpha_u^2}{R_{uu}^4}\right) - \frac{2}{R_{us}}\left(1 - \frac{\alpha_u + \alpha_s}{R_{us}^2} + \frac{3\alpha_u\alpha_s}{R_{us}^4}\right) + \frac{1}{R_{ss}}\left(1 - \frac{2\alpha_s}{R_{ss}^2} + \frac{3\alpha_s^2}{R_{ss}^4}\right)\right], \tag{35}$$

$$(\Delta E_{\Sigma^0})_g^M = \frac{256\alpha_c}{9\sqrt{\pi}}\left[\frac{1}{(3\epsilon_u' + m_u')^2 R_{uu}^3} - \frac{4}{R_{us}^3(3\epsilon_u' + m_u')(3\epsilon_s' + m_s')}\right], \tag{36}$$

$$(\Delta E_{\Sigma^0})_g = (\Delta E_{\Sigma^0})_g^E + (\Delta E_{\Sigma^0})_g^M. \tag{37}$$

The gluonic correction for Λ is

$$(\Delta E_{\Sigma^0})_g^E = (\Delta E_{\Lambda})_g^E. \tag{38}$$

The color magnetic contribution is different

$$(\Delta E_{\Lambda})_g^M = -\frac{256\alpha_c}{3\sqrt{\pi}}\left[\frac{1}{(3\epsilon_u' + m_u')^2 R_{uu}^3}\right], \tag{39}$$

$$(\Delta E_{\Lambda})_g = (\Delta E_{\Lambda})_g^E + (\Delta E_{\Lambda})_g^M. \tag{40}$$

The color electric contributions for Ξ^- and Ξ^0 are same as that of Σ^0 or Λ^0 but the color magnetic contributions to the correction of masses of baryon are different:

$$(\Delta E_{\Xi^-,\Xi^0})_g^M = \frac{256\alpha_c}{9\sqrt{\pi}}\left[\frac{1}{(3\epsilon_s' + m_s')^2 R_{ss}^3} - \frac{4}{R_{us}^3(3\epsilon_u' + m_u')(3\epsilon_s' + m_s')}\right]. \tag{41}$$

Finally, the gluonic correction for Ξ^- and Ξ^0 is given by

$$(\Delta E_{\Xi^-,\Xi^0})_g = (\Delta E_{\Xi^-,\Xi^0})_g^E + (\Delta E_{\Xi^-,\Xi^0})_g^M. \tag{42}$$

Treating all energy corrections independently, the mass of the baryon in the medium becomes

$$M_B^* = E_B^{*0} - \epsilon_{\text{c.m.}} + \delta M_B^{\pi} + (\Delta E_B)_g^E + (\Delta E_B)_g^M. \tag{43}$$

IV. THE EQUATION OF STATE

The total energy density and pressure at a particular baryon density, encompassing all the members of the baryon octet, for the nuclear matter in β equilibrium can be found as

$$\mathcal{E} = \frac{1}{2}m_\sigma^2\sigma_0^2 + \frac{1}{2}m_\omega^2\omega_0^2 + \frac{1}{2}m_\rho^2 b_{03}^2 + 3g_\omega^2 g_\rho^2 \Lambda_\nu b_{03}^2\omega_0^2 + \frac{\gamma}{2\pi^2}\sum_B \int^{k_{f,B}} \left[k^2 + M_B^{*2}\right]^{1/2} k^2 dk + \sum_l \frac{1}{\pi^2}\int_0^{k_l} \left[k^2 + m_l^2\right]^{1/2} k^2 dk, \tag{44a}$$

$$P = -\frac{1}{2}m_\sigma^2\sigma_0^2 + \frac{1}{2}m_\omega^2\omega_0^2 + \frac{1}{2}m_\rho^2 b_{03}^2 + g_\omega^2 g_\rho^2 \Lambda_\nu b_{03}^2\omega_0^2 + \frac{\gamma}{6\pi^2}\sum_B \int^{k_{f,B}} \frac{k^4 dk}{\left[k^2 + M_B^{*2}\right]^{1/2}} + \frac{1}{3}\sum_l \frac{1}{\pi^2}\int_0^{k_l} \frac{k^4 dk}{\left[k^2 + m_l^2\right]^{1/2}}, \tag{44b}$$

where $\gamma = 2$ is the spin degeneracy factor for nuclear matter, $B = N, \Lambda, \Sigma^\pm, \Sigma^0, \Xi^-, \Xi^0$, and $l = e, \mu$. In the above expression for the energy density and pressure, a nonlinear ω-ρ coupling term is introduced with coupling coefficient, Λ_ν [39].

Another important quantity for the study of nuclear matter is the symmetry energy, which is defined as

$$\mathcal{E}_{\text{sym}}(\rho_B) = \frac{k^2}{6E_N^{*2}} + \frac{g_\rho^2}{8m_\rho^2}\rho_B, \tag{45}$$

TABLE II. The potential parameter V_0 obtained for the quark mass $m_u = m_d = 80$ MeV, $m_s = 230$ MeV with $a = 0.81006$ fm^{-3} and the quark mass $m_u = m_d = 150$ MeV, $m_s = 300$ MeV with $a = 0.69655$ fm^{-3}. Also shown are the contribution of the center of mass correction, pionic correction, and gluonic correction to the baryon mass in free space.

Baryon	M_B (MeV)	$m_q = 80$ MeV				$m_q = 150$ MeV			
		V_0 (MeV)	$e_{\text{c.m.}}$ (MeV)	δ_B^π (MeV)	$(\Delta E_B)_g$ (MeV)	V_0 (MeV)	$e_{\text{c.m.}}$ (MeV)	δ_B^π (MeV)	$(\Delta E_B)_g$ (MeV)
N	939	82.93	357.92	−72.52	−68.69	44.05	331.84	−86.96	−59.02
Λ	1115.6	87.03	317.80	−46.43	−65.34	50.06	310.39	−55.82	−56.13
Σ	1193.1	105.27	316.16	−27.36	−52.87	66.44	308.84	−32.38	−45.00
Ξ	1321.3	114.43	319.79	−12.67	−57.65	66.82	302.17	−14.58	−49.64

where $E_N^* = \sqrt{k^2 + M_N^{*2}}$, the index $N = n, p$ for neutrons and protons. The slope of the symmetry energy L is then obtained as

$$L = 3\rho_0 \frac{\partial \mathcal{E}_{\text{sym}}(\rho_B)}{\partial \rho_B}\bigg|_{\rho_B=\rho_0}. \tag{46}$$

For obtaining a constraint on the quark mass we use the value of compressibility given by

$$K = 9\left[\frac{dP}{d\rho_B}\right]_{\rho_B=\rho_0} \tag{47}$$

The chemical potentials, necessary to define the $\beta-$ equilibrium conditions, are given by

$$\mu_B = \sqrt{k_B^2 + M_B^{*2}} + g_\omega \omega_0 + g_\rho \tau_{3B} b_{03}, \tag{48}$$

where τ_{3B} is the isospin projection of the baryon B.

The lepton Fermi momenta are the positive real solutions of $(k_e^2 + m_e^2)^{1/2} = \mu_e$ and $(k_\mu^2 + m_\mu^2)^{1/2} = \mu_\mu$. The equilibrium composition of the star is obtained by solving the equations of motion of meson fields in conjunction with the charge neutrality condition, given in Eq. (50), at a given total baryonic density $\rho = \sum_B \gamma k_B^3/(6\pi^2)$. The effective masses of the baryons are obtained self-consistently in this model.

Since we consider the octet baryons, the presence of strange baryons in the matter plays a significant role. We define the strangeness fraction as

$$f_s = \frac{1}{3}\frac{\sum_i |s_i|\rho_i}{\rho}. \tag{49}$$

Here s_i refers to the strangeness number of baryon i and ρ_i is defined as $\rho_i = \gamma k_{Bi}^3/(6\pi^2)$.

For stars in which the strongly interacting particles are baryons, the composition is determined by the requirements of charge neutrality and β-equilibrium conditions under the weak processes $B_1 \to B_2 + l + \overline{\nu}_l$ and $B_2 + l \to B_1 + \nu_l$. After deleptonization, the charge neutrality condition yields

$$q_{\text{tot}} = \sum_B q_B \frac{\gamma k_B^3}{6\pi^2} + \sum_{l=e,\mu} q_l \frac{k_l^3}{3\pi^2} = 0, \tag{50}$$

where q_B corresponds to the electric charge of baryon species B and q_l corresponds to the electric charge of lepton species l. Since the time scale of a star is effectively infinite compared to the weak interaction time scale, weak interaction violates strangeness conservation. The strangeness quantum number is therefore not conserved in a star and the net strangeness is determined by the condition of β equilibrium which for baryon B is then given by $\mu_B = b_B\mu_n - q_B\mu_e$, where μ_B is the chemical potential of baryon B and b_B its baryon number. Thus the chemical potential of any baryon can be obtained from the two independent chemical potentials μ_n and μ_e of neutron and electron, respectively.

The hyperon couplings are not relevant to the ground state properties of nuclear matter, but information about them can be available from the levels in Λ hypernuclei [40]:

$$g_{\sigma B} = x_{\sigma B} g_{\sigma N}, \quad g_{\omega B} = x_{\omega B} g_{\omega N}, \quad g_{\rho B} = x_{\rho B} g_{\rho N},$$

and $x_{\sigma B}$, $x_{\omega B}$, and $x_{\rho B}$ are equal to 1 for the nucleons and acquire different values in different parametrizations for the other baryons. We note that the s quark is unaffected by the σ and ω mesons, i.e., $g_\sigma^s = g_\omega^s = 0$.

The vector mean-fields ω_0 and b_{03} are determined through

$$\omega_0 = \frac{g_\omega}{m_\omega^{*2}} \sum_B x_{\omega B}\rho_B \quad b_{03} = \frac{g_\rho}{2m_\rho^{*2}} \sum_B x_{\rho B}\tau_{3B}\rho_B, \tag{51}$$

where $m_\omega^{*2} = m_\omega^2 + 2\Lambda_v g_\rho^2 g_\omega^2 b_{03}^2$, $m_\rho^{*2} = m_\rho^2 + 2\Lambda_v g_\rho^2 g_\omega^2 \omega_0^2$, $g_\omega = 3g_\omega^q$, and $g_\rho = g_\rho^q$. Finally, the scalar mean-field σ_0 is

TABLE III. The contribution of the center of mass correction, pionic correction, and gluonic correction to the effective mass M_B^* of the baryon at saturation density for quark mass $m_u = m_d = 80$ MeV, $m_s = 230$ MeV and $m_u = m_d = 150$ MeV, $m_s = 300$ MeV.

Baryon	$m_q = 80$ MeV				$m_q = 150$ MeV			
	M_B^* (MeV)	$e_{\text{c.m.}}$ (MeV)	δ_B^π (MeV)	$(\Delta E_B)_g$ (MeV)	M_B^* (MeV)	$e_{\text{c.m.}}$ (MeV)	δ_B^π (MeV)	$(\Delta E_B)_g$ (MeV)
N	834.03	364.64	−35.40	−77.84	797.29	344.38	−46.13	−69.39
Λ	1039.49	326.18	−46.45	−48.29	1018.10	322.28	−57.05	−33.28
Σ	1109.39	324.65	−27.47	−40.59	1087.53	320.77	−33.17	−28.47
Ξ	1289.59	322.88	−12.74	−41.86	1282.12	307.00	−14.94	−28.92

TABLE IV. Parameters for nuclear matter. They are determined from the binding energy per nucleon, $E_{B.E} = B_0 \equiv \mathcal{E}/\rho_B - M_N = -15.7$ MeV and pressure, $P = 0$ at saturation density $\rho_B = \rho_0 = 0.15$ fm^{-3}. Also shown are the values of the nuclear matter incompressibility K and the slope of the symmetry energy L for the quark masses $m_q = 80$ MeV and $m_q = 150$ MeV.

m_q (MeV)	g_σ^q	g_ω	g_ρ			σ_0 (MeV)	M_N^*/M_N	K (MeV)	L (MeV)		
			$\Lambda_v = 0$	$\Lambda_v = 0.05$	$\Lambda_v = 0.1$				$\Lambda_v = 0$	$\Lambda_v = 0.05$	$\Lambda_v = 0.1$
80	4.89039	5.17979	8.92265	9.0790	9.2440	13.34	0.88	246	85.44	87.53	89.77
150	4.39952	6.74299	8.79976	9.2522	9.7825	14.44	0.87	292	86.39	92.45	99.95

fixed by

$$\frac{\partial \mathcal{E}}{\partial \sigma_0} = 0. \tag{52}$$

The isoscalar scalar and isoscalar vector couplings g_σ^q and g_ω are fitted to the saturation density and binding energy for nuclear matter. The isovector vector coupling g_ρ is set by fixing the symmetry energy at $J = 32.0$ MeV. For a given baryon density, ω_0, b_{03}, and σ_0 are calculated from Eqs. (51) and (52), respectively.

Following the determination of the EOS the relation between the mass and radius of a star with its central density can be obtained by integrating the Tolman-Oppenheimer-Volkoff (TOV) equations [41] given by

$$\frac{dP}{dr} = -\frac{G}{r}\frac{[\mathcal{E}+P][M+4\pi r^3 P]}{(r-2GM)}, \tag{53}$$

$$\frac{dM}{dr} = 4\pi r^2 \mathcal{E} \tag{54}$$

with G as the gravitational constant and $M(r)$ as the enclosed gravitational mass. We have used $c = 1$. Given an EOS, these equations can be integrated from the origin as an initial value problem for a given choice of the central energy density, (ε_0). Of particular importance is the maximum mass obtained from and the solution of the TOV equations. The value of $r(= R)$, where the pressure vanishes defines the surface of the star.

V. RESULTS AND DISCUSSION

Our MQMC model has two potential parameters, a and V_0 and we obtain them by fitting the nucleon mass $M_N = 939$ MeV and charge radius of the proton $\langle r_N \rangle = 0.87$ fm in free space. Keeping the value of the potential parameter a same as that for nucleons, we obtain V_0 for the Λ, Σ, and Ξ baryons by fitting their respective masses to $M_\Lambda = 1115.6$ MeV, $M_\Sigma = 1193.1$ MeV, and $M_\Xi = 1321.3$ MeV. The set of potential parameters for the baryons along with their respective energy corrections at zero density are given in Table II. The quark meson couplings g_σ^q, $g_\omega = 3g_\omega^q$, and $g_\rho = g_\rho^q$ are fitted self-consistently for the nucleons to obtain the correct saturation properties of nuclear matter binding energy, $E_{B.E.} \equiv B_0 = \mathcal{E}/\rho_B - M_N = -15.7$ MeV, pressure, $P = 0$, and symmetry energy $J = 32.0$ MeV at $\rho_B = \rho_0 = 0.15$ fm^{-3}.

Table III shows the contribution to the spurious center-of-mass correction, the pionic correction, and the gluonic correction to obtain the effective mass of the baryon. It is interesting to note that as the mass of the quark increases from 80 MeV to 150 MeV, the magnitude of the pionic correction increases whereas that due gluonic correction decreases for all baryon species.

We have taken the standard values for the meson masses; namely, $m_\sigma = 550$ MeV, $m_\omega = 783$ MeV, and $m_\rho = 763$ MeV. The values of the quark meson couplings, g_σ^q, g_ω, and g_ρ at quark masses 80 MeV and 150 MeV are given in Table IV.

By changing the value of the ω-ρ coupling term Λ_v there is a change in the value of g_ρ. For $\Lambda_v = 0.05$ and 0.1 we obtain the values of g_ρ to be 9.25223 and 9.78255, respectively.

Incompressibility K of symmetric nuclear matter as well as the slope of the symmetry energy L provide important constraints to the properties of nuclear matter. In the present work, we determine the value of the compression modulus K at quark masses 80 MeV and 150 MeV which comes out to be 246 MeV and 292 MeV, respectively. From various experimental giant monopole resonance (GMR) studies [37] and microscopic calculations of the GMR energies [42] the value of K is predicted to lie in the range $250 < K < 325$ MeV and 230 ± 40 MeV, respectively. The slope of the nuclear symmetry energy L in the present work is calculated to be 85.44 MeV and 86.39 MeV for quark masses 80 MeV and 150 MeV, which agrees well with the value 88 ± 25 extracted from isospin sensitive observables in heavy-ion reactions [43]. By increasing the value of Λ_v the value of L increases to $L = 92.45$ for $\Lambda_v = 0.05$ and $L = 99.95$ for $\Lambda_v = 0.1$. The couplings of the hyperons to the σ meson need not be fixed since we determine the effective masses of the hyperons self-consistently. The hyperon couplings to the ω meson are fixed by determining $x_{\omega B}$. The value of $x_{\omega B}$ is obtained from the hyperon potentials in nuclear matter, $U_B = -(M_B - M_B^*) + x_{\omega B} g_\omega \omega_0$ for $B = \Lambda, \Sigma$, and Ξ as -28 MeV, 30 MeV, and -18 MeV, respectively. For the

TABLE V. $x_{\omega B}$ determined by fixing the potentials for the hyperons.

m_q (MeV)	$x_{\omega\Lambda}$	$x_{\omega\Sigma}$	$x_{\omega\Xi}$		
	$U_\Lambda = -28$ MeV	$U_\Sigma = 30$ MeV	$U_\Xi = -18$ MeV	$U_\Xi = -10$ MeV	$U_\Xi = 0$ MeV
80	0.95375	2.25435	0.27168	0.43029	0.62857
150	0.81309	1.58607	0.24769	0.34129	0.45829

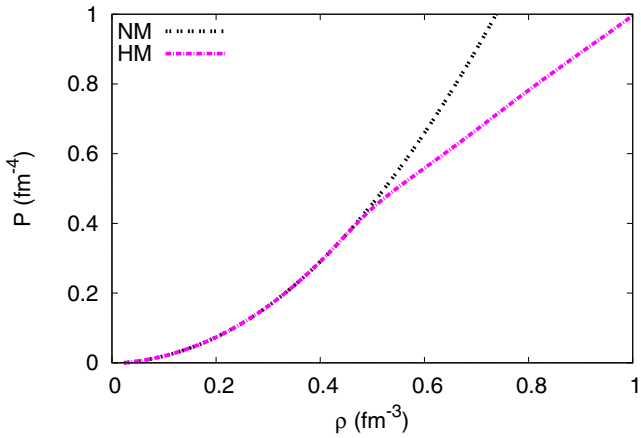

FIG. 1. The pressure at various densities for nuclear matter (NM) and hyperon matter (HM).

quark masses 80 MeV and 150 MeV the corresponding values for $x_{\omega B}$ are given in Table V. The value of $x_{\rho B} = 1$ is fixed for all baryons.

The Λ hyperon potential has been chosen from the measured single particle levels of Λ hypernuclei from mass numbers $A = 3$ to 209 [44] of the binding of Λ to symmetric nuclear matter. Studies of Σ nuclear interaction [45,46] from the analysis of Σ^- atomic data indicate a repulsive isoscalar potential in the interior of nuclei. However, measurements of the Ξ hyperon potential exhibit uncertainties. Measurements of the final state interaction of Ξ hyperons produced in (K^-, K^+) reaction on ^{12}C in E224 experiment at KEK [47] and E885 experiment at AGS [48] indicate a shallow attractive potential $U_\Xi \sim -16$ MeV and $U_\Xi \sim -14$ or less, respectively. Hence, to study the effect of the coupling to the cascade we show the results at $U_\Xi = -10$ MeV and $U_\Xi = 0$ MeV in addition to $U_\Xi = -18$ MeV. For $U_\Xi = -10$ MeV $x_{\omega\Xi} = 0.43029$ at $m_q = 80$ MeV and $x_{\omega\Xi} = 0.34129$ at $m_q = 150$ MeV. For $U_\Xi = 0$ MeV $x_{\omega\Xi} = 0.62857$ at $m_q = 80$ MeV and $x_{\omega\Xi} = 0.45829$ at $m_q = 150$ MeV. The effect of including hyperons in neutron star matter is shown in Fig. 1. It is observed that the EOS of neutron star matter with hyperons becomes softer

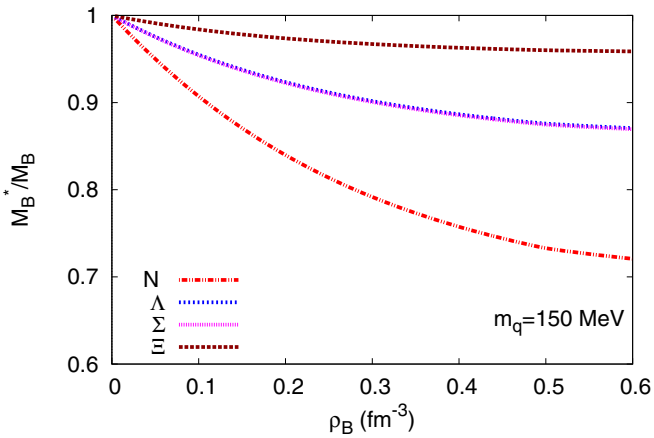

FIG. 2. Effective mass of baryon at quark mass $m_q = 150$ MeV.

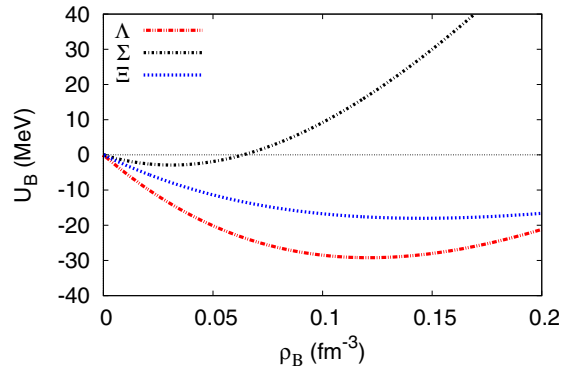

FIG. 3. Hyperon (Λ, Σ, Ξ) potentials as a function of density.

starting from density $\rho_B = 0.49$ fm^{-3} compared to the one without the hyperons. The reason for such behavior is that at $\rho_B = 0.49$ fm^{-3} corresponding to $P \geqslant 86.2$ MeV/fm^{-3} or $P = 0.437$ fm^{-4} of neutron star matter, slow moving Λ, Σ, and Ξ hyperons appear and the number of energetic nucleons and leptons decreases.

Figure 2 shows the effective baryon mass, M_B^*/M_B, as a function of baryon density. At saturation density ρ_0 the value of M_B^*/M_B increases from 0.87 for nucleons to 0.97 for the Ξ baryon. With increase in baryon density the effective mass decreases and then saturates at high baryon densities.

The potentials that we have fixed for Λ, Σ, and Ξ hyperons are plotted in Fig. 3. The hyperon potentials reduce with increasing density due to stronger repulsive effect at higher densities. In fact all hyperon potentials become repulsive nearly after twice the saturation density due to the nonlinear density dependence of the baryon potentials.

In Fig. 4 we plot the equation of state for quark mass $m_q = 150$ MeV at different values of the coupling parameter Λ_v. The shaded region shows the empirical EOS obtained by Steiner *et al.* from a heterogeneous set of seven neutron stars with well determined distances [49]. We also show, for comparison,

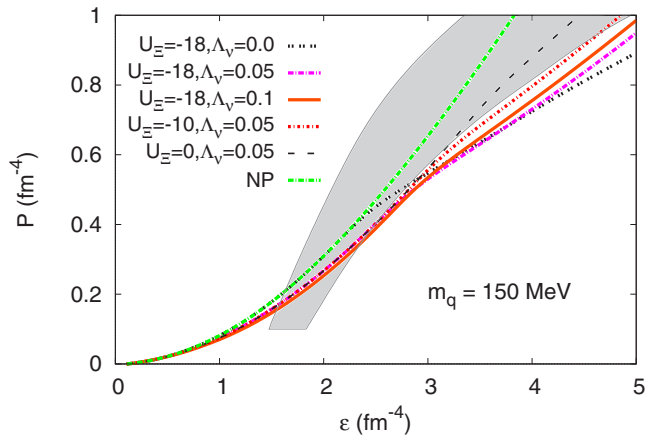

FIG. 4. The EOS at various cascade potentials and different values of Λ_v for quark mass $m_q = 150$ MeV. The shaded region shows the empirical EOS obtained by Steiner *et al.* from a heterogeneous set of seven neutron stars.

TABLE VI. Stellar properties obtained at different values of the parameter Λ_v and the Ξ-meson coupling for quark mass $m_q =$ 80 MeV and $m_q = 150$ MeV.

m_q (MeV)	U_Ξ (MeV)	Λ_v	ε_0 (fm^{-4})	$M_{\max}$ ($M_\odot$)	R (km)	$R_{1.4}$ (km)
80	−18	0	4.37	1.81	13.9	16.4
	−18	0.05	4.65	1.70	13.6	16.0
	−18	0.1	4.98	1.64	13.2	15.5
	−10	0	4.73	1.85	13.6	16.4
	0	0	5.24	1.88	13.1	16.4
150	−18	0	3.52	2.15	15.6	19.2
	−18	0.05	3.99	2.00	14.9	19.1
	−18	0.1	4.38	1.95	14.4	18.8
	−10	0	3.75	2.18	15.2	19.2
	−10	0.05	4.28	2.03	14.6	19.1
	−10	0.1	4.66	1.98	14.1	18.9
	0	0	4.03	2.21	14.9	19.2
	0	0.05	4.64	2.05	14.1	18.9
	0	0.1	5.07	2.01	13.7	18.8

the EOS without the hyperons. The EOS with only neutron and proton (NP) matter is the stiffest and the corresponding star mass for quark mass $m_q = 150$ MeV is 2.25 $M_\odot$. The EOS with hyperons is softer than with NP matter. In fact, the softness increases by fixing the hyperon nuclear potentials at $U_\Lambda = -28$ MeV, $U_\Sigma = 30$ MeV, and $U_\Xi = -18$ MeV. Within such a set of potentials we observe that by increasing the coupling parameter Λ_v the softness of the EOS increases with a corresponding decrease in radius. The effect of the variation in the values of the coupling parameter Λ_v on the star mass and radius is given in Table VI. By changing Λ_v from 0 to 0.1 the radius decreases by ∼1.2 km and the mass of the star decreases by 0.2 $M_\odot$. The variation in the softness with change in cascade potential U_Ξ is studied. We observe that the EOS becomes stiffer for less attractive U_Ξ. Consequently we see that the mass increases by $0.06 M_\odot$ if U_Ξ increases from −18 to 0 MeV. This can be attributed to the fact that the hyperons occur at higher densities. For a comparison, we also show in Table VI the radius corresponding to the canonical mass of 1.4 $M_\odot$.

Figure 5 shows the particle fractions for various fits of the cascade potential U_Ξ in β-equilibrated matter. At densities below the saturation value the β decay of neutrons to muons are allowed and thus muons start to populate. At higher densities the lepton fraction begins to fall since charge neutrality can now be maintained more economically with the appearance of negative hyperon species. In the present case we observe the appearance of Ξ^- first followed by Λ baryon. Such a trend seems to be associated with our fittings of the cascade potential. At high densities all baryons tend to saturate. Given the growth of hyperons at higher densities, the dense interior of the star resembles more to a hyperon star than a neutron star.

Moreover, the Σ hyperon is not present in the matter distribution for the given set of potentials since we have chosen a repulsive potential for it. The lepton fractions begin to drop at around $3\rho_0$. Hence to balance the positive charge of the protons the negatively charged Ξ^- appear. It may be noted

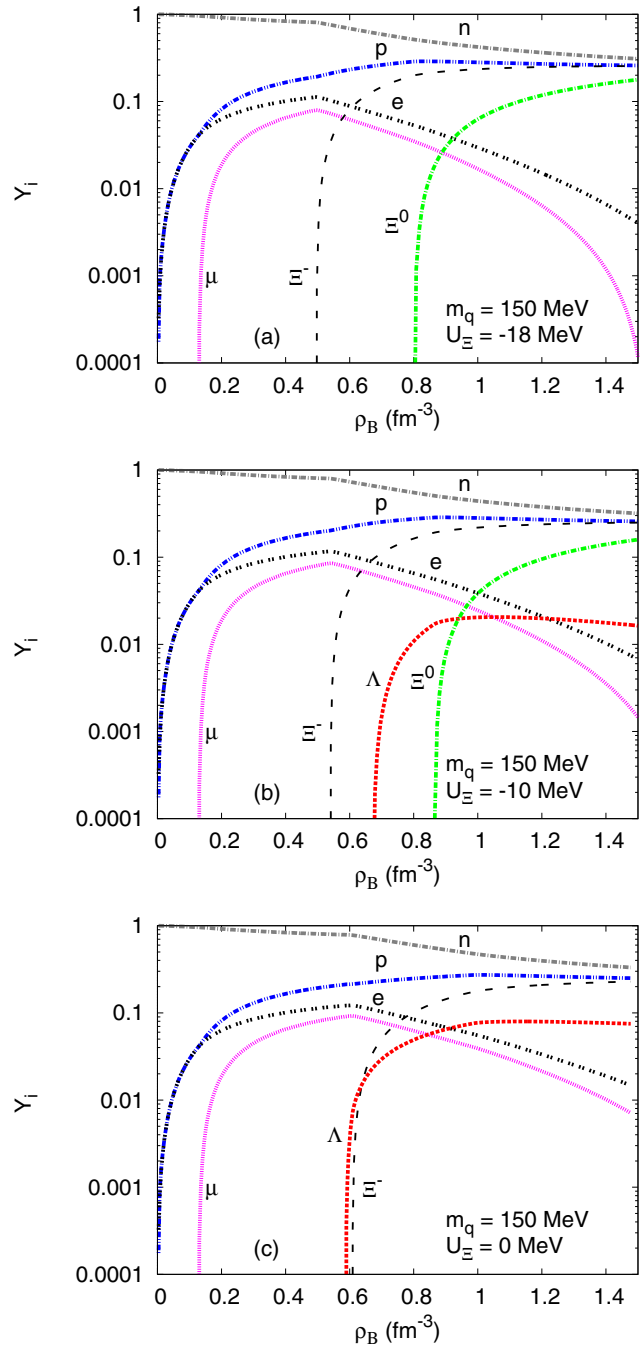

FIG. 5. Particle fraction at different cascade potentials of (a) $U_\Xi = -18$ MeV, (b) $U_\Xi = -10$ MeV, and (c) $U_\Xi = 0$ MeV for the quark mass $m_q = 150$ MeV.

that the contribution of repulsive vector potential to the overall potential must be larger in order to prevent a collapse of the matter. The repulsive vector potential for Ξ^- is smaller by a factor of two for other hyperons and by a factor of three for nucleons. In this light we can observe from Fig. 5 that the Ξ^- is more favored to appear.

The variation of the strangeness fraction and particle fraction of the Ξ^- with density is compared to that of the neutron in Fig. 6. The particle fraction of the Ξ^- hyperon

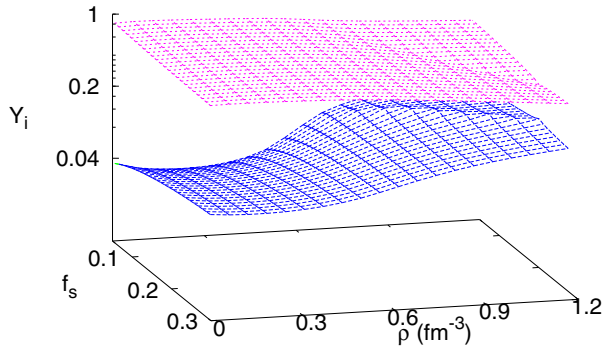

FIG. 6. Strangeness fraction and particle fraction variation with density. The upper grid is for neutron and the lower one represents Ξ^- hyperon.

increases at higher densities implying the appearance of strangeness. With increasing densities the particle fraction of the neutron decreases and tends to saturate. We should note here that the strangeness content is sensitive to the meson-hyperon couplings. This can be observed in Fig. 7. By increasing the cascade potential from $U_\Xi = -18$ MeV to $U_\Xi = 0$ MeV, the onset of hyperons occurs at higher densities. This makes the EOS stiffer for a less attractive potential.

In Fig. 8 we plot the mass-radius relations at two quark masses of $m_q = 80$ MeV and $m_q = 150$ MeV for the various scenarios and observe a direct correlation with the degree of stiffness of the EOS. As discussed earlier, for low values of the coupling parameter Λ_v the EOS is stiffer giving higher mass as compared to higher values of Λ_v. Moreover, if we vary the cascade potential, we observe that for less attractive potential, the mass is the highest giving $M_{\rm star} = 1.88 M_\odot$ for quark mass $m_q = 80$ MeV and $M_{\rm star} = 2.21 M_\odot$ at $m_q = 150$ MeV. The detailed results are shown in Table VI. The recently observed pulsar PSR J0348+0432 provide a mass constraint of $2.01 \pm 0.04 M_\odot$ [25] while an earlier accurately measured pulsar PSR J1614-2230 gives a mass of $1.97 \pm 0.04 M_\odot$ [24]. From our calculations we obtain a range of masses varying from $1.95 M_\odot$ to $2.21 M_\odot$ depending on the values of the coupling term as

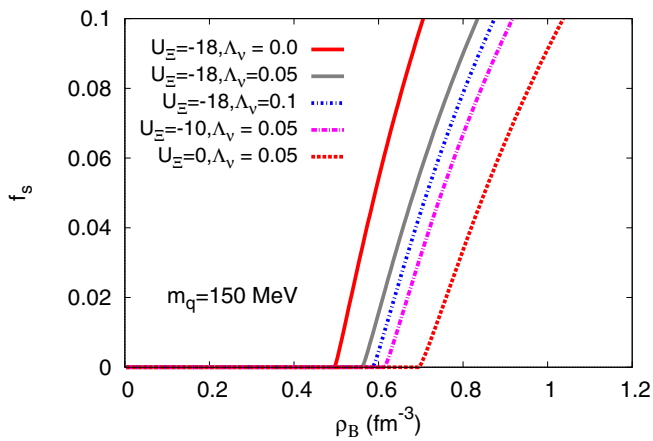

FIG. 7. Strangeness fraction as a function of density for various cascade potentials.

well as the variation of the cascade potential. The neutron star mass has been obtained under a similar framework in QMC using bag model with variation in the values of Λ_v and the cascade potential [50]. In this model the star mass obtained for the fixed cascade potential of -18 MeV gives a value 1.776 $M_\odot$, 1.880 $M_\odot$, and 1.888 $M_\odot$ for $\Lambda_v = 0, 0.05$, and 0.1, respectively.

Though the measurement of the mass of the pulsars PSR J0348+0432 and PSR J1614-2230 is precise, the corresponding radii measurements are not available. In fact, the simultaneous measurement of mass and radius of the same stellar object is uncertain. Radius measurements are primarily carried out from the studies of bursting neutron stars that show photospheric radius expansion [51] and from transiently accreting neutron stars in quiescence [52]. Results from such measurements have been used to infer the pressure at several fiducial densities [53–55] as well as to put constraints on the neutron star equation of state at high densities [56]. A recent study [26] involving radius measurements to develop a neutron star equation of state predicts the radius to be 10.1–11.1 km for a star of mass $M = 1.5 M_\odot$. Another analysis [57] encompassing variations in EOS and interpretations of the astrophysical data predicts the radius of a $M = 1.4 M_\odot$ neutron star to lie between 10.4 km and 12.9 km. In the present work the radius corresponding to the canonical mass of $1.4 M_\odot$ is between 15.5–16.4 km for $m_q = 80$ MeV and between 18.8–19.2 for $m_q = 150$ MeV, which is quite higher than the radius range of 10.7–13.1 km for $M = 1.4 M_\odot$ stars [58–60] obtained from nuclear experimental studies. One of the reasons for this discrepancy on the radius may be due to the fact that the EOS considered here for the TOV equation does not include at high density, the effects of other phases of matter such as quark matter, mixed matter or paired quark matter. However within the context of the present model, an improvement on this result may be explained by introducing additional interactions through δ, σ^*, and ϕ meson exchanges without taking any other nonlinear interactions.

VI. CONCLUSION

In the present work we have developed the EOS using a modified quark-meson coupling model which considers the baryons to be composed of three independent relativistic quarks confined by an equal admixture of a scalar-vector harmonic potential in a background of scalar and vector mean fields. Corrections to the center of mass motion, pionic, and gluonic exchanges within the nucleon are calculated to obtain the effective mass of the baryon. The baryon-baryon interactions are realized by the quark coupling to the σ, ω, and ρ mesons through a mean field approximation. The nuclear matter incompressibility K is determined to agree with experimental studies. Further, the slope of the nuclear symmetry is calculated which also agrees well with experimental observations.

The EOS is analyzed for different values of the nonlinear coupling Λ_v and quark mass. The variation in the degree of softness or stiffness of the EOS is concluded to be directly related to the higher or lower values of the coupling Λ_v and

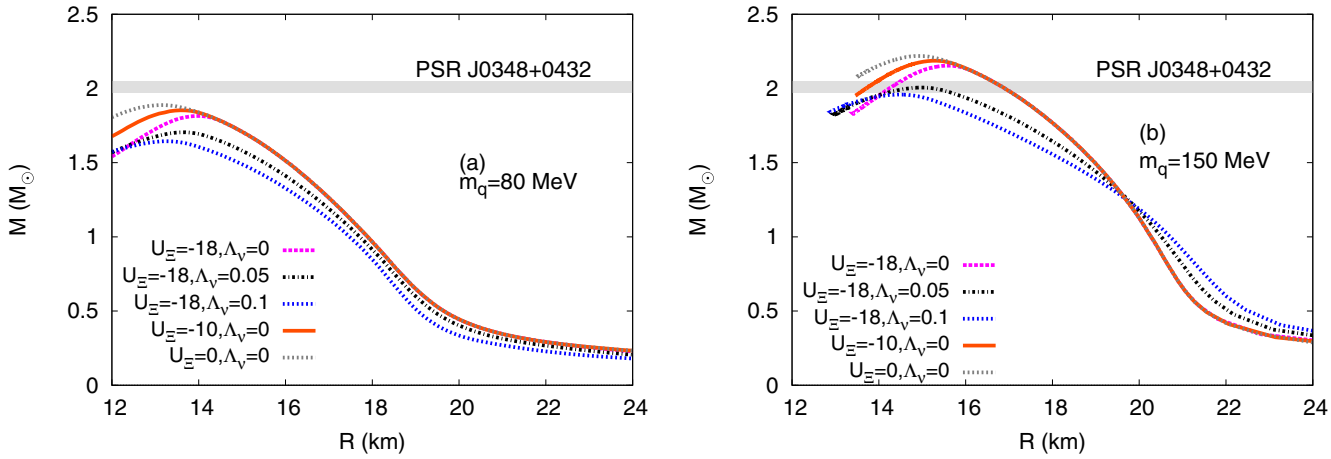

FIG. 8. Star mass as a function of radius for various values of the coupling parameter and cascade potential at quark masses (a) $m_q = 80$ MeV and (b) $m_q = 150$ MeV. Also shown is the mass observed for the pulsar PSR J0348+0432 in [25].

quark mass m_q. The increase in the value of the coupling Λ_v softens the EOS and decreases the maximum mass of star. In fact, we observe that there is no significant advantage of such a term in the context of obtaining the star mass constraint in the present set of parametrizations.

By increasing the quark mass the scalar coupling tends to be less sensitive to density variations, i.e., decreases more slowly and to fit to the nuclear matter properties more repulsion is required. The maximum star mass and strangeness fraction are quite sensitive to that, being larger/smaller by increasing/decreasing the quark mass. Further, by fixing the hyperon-ω coupling from information of the hypernuclei as well as increasing the potential U_Ξ to make it less attractive we have analyzed the variation in the stiffness of the EOS and the strangeness fraction at higher densities. We observe that the hyperon interactions influence the amount of strangeness in the star and thus have a strong impact on the maximum mass. We were able to obtain the observed mass of two accurately calculated pulsars, namely, PSR J0348+0432 and PSR J1614-2230 by varying the quark mass and cascade potentials, but more information on hypernuclei is required to further streamline the hyperon-meson couplings, such that we can constrain the quark mass parameter and strangeness fraction in the star.

In the present set of parametrization, although we get the mass of the neutron star within the constraint of 2 $M_\odot$, the radius corresponding to the canonical mass of 1.44 $M_\odot$ is beyond the predicted values. From the studies of the effects of symmetry energy and strangeness content on neutron stars, Providência and Rabhi [28] observe that the radius of a hyperonic star of a given mass decreases linearly with the increase of the total hyperon content. By incorporating δ, σ^*, and ϕ meson exchange contributions, we may expect some improvement in the prediction of the radius. Work in this direction is in progress.

ACKNOWLEDGMENTS

The authors would like to acknowledge the financial assistance from DAE-BRNS, India for Project No. 2013/37P/66/BRNS. T.F. thanks the support of the Brazilian agency Conselho Nacional de Desenvolvimento Científico e Tecnológico (CNPq) with Project No. 308486/2015-3.

[1] V. A. Ambartsumyan and G. S. Saakyan, Sov. Astron. **4**, 187 (1960).
[2] P. Ring, Prog. Part. Nucl. Phys. **37**, 193 (1996).
[3] A. Akmal, V. R. Pandharipande, and D. G. Ravenhall, Phys. Rev. C **58**, 1804 (1998).
[4] J. R. Stone and P. G. Reinhard, Prog. Part. Nucl. Phys. **58**, 587 (2007).
[5] J. R. Stone *et al.*, Nucl. Phys. A **792**, 341 (2007).
[6] F. Weber, Prog. Part. Nucl. Phys. **54**, 193 (2005).
[7] W. Weise, Prog. Part. Nucl. Phys. **67**, 299 (2012).
[8] B. D. Lackey, M. Nayyar, and B. J. Owen, Phys. Rev. D **73**, 024021 (2006).
[9] D. Chatterjee and I. Vidaña, Eur. Phys. J. A **52**, 29 (2016).
[10] N. Glendenning, Astrophys. J. **293**, 470 (1985).
[11] N. K. Glendenning and S. A. Moszkowski, Phys. Rev. Lett. **67**, 2414 (1991); M. Hanauske, D. Zschiesche, S. Pal, S. Schramm, and W. G. H. Stocker, Astrophys. J. **537**, 958 (2000); S. Schramm and D. Zschiesche, J. Phys. G **29**, 531 (2003); W. H. Long, B. Y. Sun, K. Hagino, and H. Sagawa, Phys. Rev. C **85**, 025806 (2012).
[12] R. Knorren, M. Prakash, and P. J. Ellis, Phys. Rev. C **52**, 3470 (1995).
[13] S. Balberg and A. Gal, Nucl. Phys. A **625**, 435 (1997).
[14] M. Prakash, I. Bombaci, M. Prakash, P. J. Ellis, and J. M. Lattimer, Phys. Rep. **280**, 1 (1997).
[15] A. R. Taurines, C. A. Z. Vasconcellos, M. Malheiro, and M. Chiapparini, Mod. Phys. Lett. A **15**, 1789 (2000).
[16] T. Miyatsu, M.-K. Cheoun, and K. Saito, Phys. Rev. C **88**, 015802 (2013).

[17] T. Miyatsu, S. Yamamuro, and K. Nakazato, Astrophys. J. **777**, 4 (2013).
[18] I. Bednarek, P. Haensel, J. L. Zdunik, M. Bejger, and R. Mańka, Astron. Astrophys. **543**, A157 (2012).
[19] S. Weissenborn, D. Chatterjee, and J. Schaffner-Bielich, Phys. Rev. C **85**, 065802 (2012).
[20] W.-Z. Jiang, B.-A. Li, and L.-W. Chen, Astrophys. J. **756**, 56 (2012).
[21] D. J. Champion *et al.*, Science **320**, 1309 (2008).
[22] P. C. C. Freire, arXiv:0907.3219.
[23] P. C. C. Freire *et al.*, MNRAS **412**, 2763 (2011).
[24] P. B. Demorest *et al.*, Nature **467**, 1081 (2010).
[25] J. Antoniadis *et al.*, Science **340**, 1233232 (2013).
[26] F. Özel, D. Psaltis, T. Güver, G. Baym, C. Heinke, and S. Guillot, Astrophys. J. **820**, 28 (2016).
[27] M. Fortin, J. L. Zdunik, P. Haensel, and M. Bejger, Astron. Astrophys. **576**, A68 (2015).
[28] C. Providência and A. Rabhi, Phys. Rev. C **87**, 055801 (2013).
[29] T. Miyatsu, T. Katayama, and K. Saito, Phys. Lett. B **709**, 242 (2012); S. K. Dhiman, R. Kumar, and B. K. Agrawal, Phys. Rev. C **76**, 045801 (2007); V. Dexheimer and S. Schramm, Astrophys. J. **683**, 943 (2008).
[30] N. Barik and B. K. Dash, Phys. Rev. D **33**, 1925 (1986); **34**, 2092 (1986).
[31] N. Barik and R. N. Mishra, Phys. Rev. D **61**, 014002 (1999).
[32] P. A. M. Guichon, Phys. Lett. B **200**, 235 (1988); P. A. M. Guichon, K. Saito, E. Rodionov, and A. W. Thomas, Nucl. Phys. A **601**, 349 (1996).
[33] P. K. Panda, A. Mishra, J. M. Eisenberg, and W. Greiner, Phys. Rev. C **56**, 3134 (1997).
[34] T. Frederico, B. V. Carlson, R. A. Rego, and M. S. Hussein, J. Phys. G **15**, 297 (1989).
[35] N. Barik, R. N. Mishra, D. K. Mohanty, P. K. Panda, and T. Frederico, Phys. Rev. C **88**, 015206 (2013).
[36] R. N. Mishra, H. S. Sahoo, P. K. Panda, N. Barik, and T. Frederico, Phys. Rev. C **92**, 045203 (2015).
[37] J. R. Stone, N. J. Stone, and S. A. Moszkowski, Phys. Rev. C **89**, 044316 (2014).
[38] L. Satpathy and R. C. Nayak, *Infinite Nuclear Matter Model of Atomic Nuclei* (Lambert Academic Publishing, Germany, 2013).
[39] C. J. Horowitz and J. Piekarewicz, Phys. Rev. Lett. **86**, 5647 (2001).
[40] M. May *et al.*, Phys. Rev. Lett. **47**, 1106 (1981).
[41] J. R. Oppenheimer and G. M. Volkoff, Phys. Rev. **55**, 374 (1939); R. C. Tolman, Proc. Nat. Acad. Sci. USA **20**, 169 (1934).
[42] E. Khan and J. Margueron, Phys. Rev. C **88**, 034319 (2013).
[43] Jun Xu, Lie-Wen Chen, Bao-An Li, and Hong-Ru Ma, Phys. Rev. C **77**, 014302 (2008).
[44] D. J. Millener, C. B. Dover, and A. Gal, Phys. Rev. C **38**, 2700 (2001); Y. Yamamoto, H. Bando, and J. Zofka, Prog. Theor. Phys. **80**, 757 (1988).
[45] J. Mares, E. Friedman, A. Gal, and B. K. Jennings, Nucl. Phys. A **594**, 311 (1995).
[46] S. Bart, R. E. Chrien, W. A. Franklin, T. Fukuda, R. S. Hayano, K. Hicks, E. V. Hungerford, R. Michael, T. Miyachi, T. Nagae, J. Nakano, W. Naing, K. Omata, R. Sawafta, Y. Shimizu, L. Tang, and S. W. Wissink, Phys. Rev. Lett. **83**, 5238 (1999).
[47] T. Fukuda, A. Higashi, Y. Matsuyama, C. Nagoshi, J. Nakano, M. Sekimoto, P. Tlusty, J. K. Ahn, H. Enyo, H. Funahashi, Y. Goto, M. Iinuma, K. Imai, Y. Itow, S. Makino, A. Masaike, Y. Matsuda, S. Mihara, N. Saito, R. Susukita, S. Yokkaichi, K. Yoshida, M. Yoshida, S. Yamashita, R. Takashima, F. Takeutchi, S. Aoki, M. Ieiri, T. Iijima, T. Yoshida, I. Nomura, T. Motoba, Y. M. Shin, S. Weibe, M. S. Chung, I. S. Park, K. S. Sim, K. S. Chung, and J. M. Lee (KEK E224 Collaboration), Phys. Rev. C **58**, 1306 (1998).
[48] P. Khaustov, D. E. Alburger, P. D. Barnes, B. Bassalleck, A. R. Berdoz, A. Biglan, T. Burger, D. S. Carman, R. E. Chrien, C. A. Davis, H. Fischer, G. B. Franklin, J. Franz, L. Gan, A. Ichikawa, T. Iijima, K. Imai, Y. Kondo, P. Koran, M. Landry, L. Lee, J. Lowe, R. Magahiz, M. May, R. McCrady, C. A. Meyer, F. Merrill, T. Motoba, S. A. Page, K. Paschke, P. H. Pile, B. Quinn, W. D. Ramsay, A. Rusek, R. Sawafta, H. Schmitt, R. A. Schumacher, R. W. Stotzer, R. Sutter, F. Takeutchi, W. T. H. vanOers, K. Yamamoto, Y. Yamamoto, M. Yosoi, and V. J. Zeps (BNL E885 Collaboration), Phys. Rev. C **61**, 054603 (2000).
[49] A. W. Steiner, J. M. Lattimer, and E. F. Brown, Astrophys. J. **722**, 33 (2010).
[50] P. K. Panda, A. M. S. Santos, D. P. Menezes, and C. Providenĉia, Phys. Rev. C **85**, 055802 (2012).
[51] W. H. G. Lewin, J. van Paradijs, and R. E. Taam, Space Sci. Rev. **62**, 223 (1993).
[52] R. E. Rutledge, L. Bildsten, E. F. Brown, G. G. Pavlov, and V. E. Zavlin, Astrophys. J. **514**, 945 (1999).
[53] L. Lindblom, Astrophys. J. **398**, 569 (1992).
[54] J. M. Lattimer and M. Prakash, Astrophys. J. **550**, 426 (2001).
[55] J. S. Read, B. D. Lackey, B. J. Owen, and J. L. Friedman, Phys. Rev. D **79**, 124032 (2009).
[56] F. Özel, G. Baym, and T. Güver, Phys. Rev. D **82**, 101301 (2010).
[57] A. W. Steiner, J. M. Lattimer, and E. F. Brown, Astrophys. J. Lett. **765**, L5 (2013).
[58] W. G. Newton, M. Gearheart, J. Hooker, and B. A. Li, in *Neutron Star Crust*, edited by C. A. Bertulani and J. Piekarewicz (Nova Science Publishers, Inc., Hauppauge, NY 2011), Chap. 12.
[59] M. B. Tsang, J. R. Stone, F. Camera *et al.*, Phys. Rev. C **86**, 015803 (2012).
[60] J. M. Lattimer and Y. Lim, Astrophys. J. **771**, 51 (2013).